$Ba_4In_8Sb_{16}$: Thermoelectric Properties of a New Layered Zintl Phase with Infinite Zigzag Sb Chains and Pentagonal Tubes

Sung-Jin Kim,[†,‡] Siqing Hu,[§] Ctirad Uher,[§] and Mercouri G. Kanatzidis*[,‡]

Department of Chemistry and Center for Fundamental Materials Research Michigan State University, East Lansing, Michigan 48824, and Department of Physics, University of Michigan, Ann Arbor, Michigan 48109

Received April 26, 1999. Revised Manuscript Received August 3, 1999

A new Zintl phase $Ba_4In_8Sb_{16}$ was obtained from a direct element combination reaction of the elements in a sealed graphite tube at 700 °C, and its structure was determined by single-crystal X-ray diffraction methods. It crystallizes in the orthorhombic space group *Pnma* (No. 62) with $a = 10.166(3)$ Å, $b = 4.5239(14)$ Å, $c = 19.495(6)$ Å, and $Z = 1$. $Ba_4In_8Sb_{16}$ has a two-dimensional structure with thick corrugated $(In_8Sb_{16})^{8-}$ layers separated by Ba^{2+} ions. In the layer, $InSb_4$ tetrahedra are connected by sharing three corners and by bridging the fourth corner in such a manner that infinite pentagonal tubes are formed. The compound is a narrow band gap (∼ 0.10 eV) semiconductor and satisfies the classical Zintl rule. Band structure calculations confirm that the material is a semiconductor and indicate that it has optimized In−Sb bonding interactions. Polycrystalline ingots of $Ba_4In_8Sb_{16}$ show room-temperature electrical conductivity of 135 S/cm and a Seebeck coefficient of 70 μV/K. The thermal conductivity of $Ba_4In_8Sb_{16}$ is about 1.7 W/m·K in the temperature range 150−300 K.

Introduction

Our approach to new thermoelectric materials, using the alkali-metal polychalcogenide flux method,[1] has proven to be effective in producing new narrow band gap bismuth chalcogenide compounds.[2−4] Large varieties of unprecedented group 15 chalcogenides have been prepared with especially encouraging properties as demonstrated in $A_xBi_yQ_z$ (A = Ba, K, Cs, Q = S, Se, Te) type compounds.[4] They possess three-dimensional or two-dimensional bismuth-chalcogenide frameworks, stabilized by weakly bonded alkali-metal or alkaline-earth-metal atoms, which reside in the cavities, channels, or galleries of the framework.[5−7] It has been suggested that heavy cation "rattling" inside of cavities or channels could create ideal conditions for phonon-contributed low thermal conductivity.[8−10] The low thermal conductivity found in the above bismuth chalcogenides is attributed mainly to three factors: (a) the presence of heavy elements in the structure, (b) the relatively low symmetry and large unit cell of the compounds, and (c) the "rattling" motion of the most electropositive atoms in the structure within their cavities.

Our experience obtained with group 15 chalcogenides drew our interest in other heavy main group framework held by heavy elements. Could new materials with group 13 and 14 elements, instead of group 15 and 16, be expected to have similar structural and compositional characteristics worth exploring for thermoelectric applications? To address this question, we turned to Zintl phases with complex polyanionic frameworks. Zintl phases are built from group 13, 14, and 15 elements, and alkali or alkaline earth metals, and often possess large cages or channels.[11,12] The great majority of Zintl compounds, however, are reported to be air and mois-

* To whom correspondence should be addressed. E-mail: Kanatzid@argus.cem.msu.edu. Telephone: 517-353-0174

† Permanent address: Department of Chemistry, Ewha Woman's University, Seoul, Korea,#120−750

‡ Michigan State University.

§ University of Michigan.

(1) Kanatzidis, M. G.; Sutorik, A. C. *Prog. Inorg. Chem*. **1996**, Vol. 43, 151−265.

(2) Chung, D.-Y.; Hogan, T.; Schindler, J.; Iordanidis, L.; Brazis, P.; Kannewurf, C. R.; Chen, B.; Uher, C.; Kanatzidis, M. G. In *Thermoelectric Materials-New Directions and Approaches*; Kanatzidis, M. G., Lyon, H., Mahan, G., Tritt, T., Eds.; Materials Research Society Symposium Proceedings 478; Materials Research Society: San Francisco, CA, 1997; pp 333−344.

(3) Kanatzidis, M. G.; DiSalvo, F. J. *Thermoelectric Materials: Solid State Synthesis*; ONR Quarterly Review: ONR: Oak Ridge, TN, 1996; Vol. XXVII, pp 14−22.

(4) (a) Chung, D.-Y.; Jobic, S.; Hogan, T.; Kannewurf, C. R.; Brec, R.; Rouxel, J.; Kanatzidis, M. G. *J. Am. Chem. Soc.* **1997**, *119*, 2505−2515. (b) Kanatzidis, M. G.; McCarthy, T. J.; Tanzer, T. A.; Chen, L.-H.; Iordanidis, L.; Hogan, T.; Kannewurf, C. R.; Uher, C.; Chen, B. *Chem. Mater*. **1996**, *8*, 1465−1474. (c) Chen, B.; Uher, C.; Iordanidis, L.; Kanatzidis, M. G. *Chem. Mater.* **1997**, *9*, 1655−1658. (d) Chung, D.-Y.; Choi, K.-Y.; Iordanidis, L.; Schindler, J. L.; Brazis, P. W.; Kannewurf, C. R.; Chen, B.; Hu, S.; Uher, C.; Kanatzidis, M. G. *Chem. Mater*. **1997**, *9*, 3060−3071. (e) Iordanidis, L.; Schindler, J. L.; Kannewurf, C. R.; Kanatzidis, M. G. *J. Solid State Chem*. **1999**, *143*, 151−162. (f) *Thermoelectric Materials-The Next Generation Materials for Small-Scale Refrigeration and Powder Generation Applications*; Kanatzidis, M. G., Lyon, H. B., Mahan, G. D., Tritt, T. M., Ed.; Materials Research Society Symposium Proceedings; Materials Research Society: Boston, MA, 1998; references therein.

(5) Kaibe, H.; Tanaka, Y.; Sakata, M.; Nishida, I. *J. Phys. Chem. Solids* **1991**, *50*, 945−950.

(6) Jeon, H.-W.; Ha, H.-P.; Hyun, D.-B.; Shin, J.-D. *J. Phys. Chem. Solids* **1991**, *52*, 579−585.

(7) *CRC Handbook of Thermoelectrics*; Rowe, D. M., Ed.; CRC Press: Boca Raton, FL, 1995.

(8) Nolas, G. S.; Cohn, J. L.; Slack, G. A.; Schujman, S. B. *Appl. Phys. Lett*. **1998**, *73*, 178−180.

(9) Nolas, G. S.; Slack, G. A.; Morelli, D. T.; Tritt, T. M.; Ehrlich, A. C. *J. Appl. Phys*. **1996**, *79*, 4002−4008.

(10) Sales, B. C. *Curr. Opin. Solid State Mater*. **1997**, *2*, 284−289.

10.1021/cm990237y CCC: $18.00
Published on Web 10/15/1999

ture sensitive. For thermoelectric applications air- and moisture-stable compounds are necessary, and this maybe achieved with the use of heavier elements and divalent electropositive cations. Recently, air-stable new Zintl frameworks were found in the ternary antimonides $Ba_2Sn_3Sb_6$ and $SrSn_3Sb_4$.[13] The structures of $Ba_2Sn_3Sb_6$ and $SrSn_3Sb_4$ are closely related; that is, both compounds form 30-membered rings and are constructed from an anionic framework of linked $SnSb_4$ tetrahedra $SnSb_3$ trigonal pyramids, and zigzag Sb−Sb chains. If heavy element analogues of the Zintl phases are synthesized, they are expected to be narrow-gap semiconductors and may have interesting thermoelectric properties. Also, recently, clathrate−I structure A_8X_{46} members (A = alkali or alkaline earth metal; X = group 12, 13, 14 elements), some of which may obey the Zintl rule, have received attention due to their pentagonal dodecahedral cages filled with cation rattlers inside.[8,9]

Attempts to synthesize new clathrate-type Zintl phases with a narrow band gap resulted in the discovery of $Ba_4In_8Sb_{16}$, which possesses an unprecedented two-dimensional network structure and infinite zigzag Sb chains. In this paper, we describe the synthesis, crystal structure, spectroscopic properties, and electronic structure of this compound. In addition, a preliminary assessment of its thermoelectric properties, including electrical conductivity, thermopower, and thermal conductivity as a function of temperature is reported.

Experimental Section

Synthesis. $Ba_4In_8Sb_{16}$ was first identified in reactions intended to synthesize a new clathrate type analogue with $Ba_8In_{16}Sb_{30}$ composition. The crystal used in the structure determination resulted from the reaction of a mixture of three elements (Ba, Aldrich, chunk under oil, 99%; In, Cerac, shots, 99.999%; Sb, Cerac, chips, 99.999%) in a molar ratio of 8:16:30. The reaction mixture was placed in a graphite tube and sealed in an evacuated quartz tube. The sealed mixture was heated slowly up to 700 °C, kept at that temperature for 1 day, and subsequently cooled to room temperature over 1 day. The reaction led to the formation of a few bar-shaped black crystals along with gray featureless pieces. Semiquantitative microprobe analysis on single crystals gave $Ba_{4.3(2)}In_{8.0(2)}Sb_{16.3(2)}$ (average of three data acquisitions). Once the stoichiometry was determined from the X-ray single-crystal structure analysis, $Ba_4In_8Sb_{16}$ was prepared rationally as a single phase, starting from the exact stoichiometric ratio. The X-ray powder pattern of bulk sample agreed well with the powder pattern calculated from single-crystal data.

Electron Microscopy. Semiquantitative microprobe analysis of the compounds was performed with a JEOL JSM-35C scanning electron microscope (SEM) equipped with a Tracor Northern Energy dispersive spectroscopy (EDS) detector. Data were acquired using an accelerating voltage of 20 kV.

Differential Thermal Analysis. Differential thermal analysis (DTA) was performed with a Shimadzu DTA-50 thermal analyzer. The ground sample (≈20.0 mg of total mass) was sealed in a carbon-coated quartz ampule under vacuum. A quartz ampule containing alumina of equal mass was sealed and placed on the reference side of the detector. The sample was heated to 950 °C at 10 °C/min and held for 10 min, followed by cooling at −10 °C/min to 50 °C. The stability and reproducibility of the sample was monitored by running multiple heating and cooling cycles. The residue of the DTA experiment was examined with X-ray powder diffraction.

Infrared Spectroscopy. Infrared diffuse reflectance spectra of $Ba_4In_8Sb_{16}$ were recorded to determine the presence of a band gap. The sample was ground into a powder prior to the data acquisition. The spectra were recorded in the mid-IR region (4000−400 cm^{-1}, 4 cm^{-1} resolution) with a Nicolet 740 FT-IR spectrometer equipped with a diffused reflectance attachment. Absorbance values were calculated from the reflectance data using the Kubelka−Munk function α/S.[14] The band gap E_g was extracted from the $(\alpha/S)^2$ vs energy plot.

Charge-Transport and Thermal Conductivity Measurements. The electrical conductivity of a polycrystalline ingot of $Ba_4In_8Sb_{16}$ was measured using the four-probe method. The polycrystalline ingot was obtained from a graphite reaction container and ground to a cylindrical shape with ∼3 mm radius and 7 mm length for measurements. Thermal conductivity and thermopower were determined using a longitudinal steady-state method over the temperature range 4−300 K. In this case samples were attached (using either a low melting point solder or silver-loaded epoxy) to the cold tip of the cryostat, while the other end of the sample was provided with a small strain gauge resistor (thin film) which serves as a heater. The temperature difference across the sample was measured using a differential chromel−constantan thermocouple.

Electronic Structure Calculations. Electronic structure calculations were performed by the Hückel method within the framework of the tight-binding approximation.[15a] The program CASEAR written by M.-H. Whangbo for IBM-compatible PC was used.[15b] Density of states (DOS) and crystal orbital overlap populations (COOP) were calculated based on 516k point sets based on the primitive orthorhombic structure. The atomic orbital parameters employed in the calculations were default values in the CASEAR program.[15b]

Crystallographic Studies. A black bar-shaped crystal with dimensions 0.03 × 0.02 × 0.30 mm was mounted on a glass fiber. A Siemens SMART Platform CCD diffractometer was used to collect intensity data using graphite monochromatized Mo Kα radiation. The data were collected over a full sphere of reciprocal space up to 56° in 2θ. The individual frames were measured with an ω rotation of 0.3° and an acquisition time of 60 s. To check the stability of the crystal, at the end of the data collection procedure, the initial 50 frames of data were measured again and compared. No crystal decay was detected. The SMART software[16] was used for data acquisition and SAINT[17] for data extraction and reduction. The absorption correction was performed empirically using SADABS.[18] The unit cell parameters were obtained from least-squares refinement using randomly chosen 600 reflections from a full sphere of reciprocal space up to 56° in 2θ. The orthorhombic cell parameters and calculated volume were a = 10.166(3) Å, b = 4.5239(14) Å, c = 19.495(6) Å, and V = 896.6(5) Å^3. The observed Laue symmetry and systematic absences were indicative of the space groups $Pnma$ or $Pn2_1a$. The centrosymmetric $Pnma$ was assumed, and subsequent refinements confirmed the choice of this space group. The

(11) (a) Vaughey, J. T.; Corbett, J. D. *J. Am. Chem. Soc.* **1996**, *118*, 12098. (b) Vaughey, J. T.; Corbett, J. D. *Inorg. Chem.* **1997**, *36*, 4316−4320. (c) Zhao, J.-T.; Corbett, J. D. *Inorg. Chem.* **1994**, *33*, 5721−5726. (d) Fässler, T. F.; Kronseder, C. *Z. Anorg. Allg. Chem.* **1998**, *624*, 561−568.

(12) (a) Eisenmann, B.; Schafer, H.; Zagler, R. *J. Less-Common Met.* **1986**, *118*, 43−55. (b) Kuhl, B.; Czybulka, A.; Schuster, H.-U. *Z. Anorg. Allg. Chem.* **1995**, *621*, 1−6. (c) Czybulka, A.; Kuhl, B.; Schuster, H.-U. *Z. Anorg. Allg. Chem.* **1991**, *594*, 23−28. (d) Dünner, J.; Mewis, A. *Z. Anorg. Allg. Chem.* **1995**, *621*, 191−196.

(13) (a) Chow, D. T.; McDonald, R.; Mar, A. *Inorg. Chem.* **1997**, *36*, 3750−3753. (b) Lam, R.; Mar, A. *Inorg. Chem.* **1996**, *35*, 6959−6963.

(14) Pankove, J. I. *Optical Process in Semiconductors*; Dover Publication: New York, 1976.

(15) (a) Hoffman, R. *J. Chem. Phys.* **1963**, *39*, 1397. (b) Canadell, E.; Whangbo, M.-H., *Chem. Rev.* **1991**, *91*, 965. (b) Ren, J.; Liang, W.; Whangbo, M.-H. Primecolor Software, Inc. Cary, NC.

(16) SMART: Siemens Analytical X-ray System, Inc., Madison, WI, 1994.

(17) SAINT, Version4: Siemens Analytical X-ray System, Inc., Madison, WI, 1994−1996.

(18) Sheldrick, G. M. University of Göttingen, Germany, to be published.

Table 1. Selected Data from the Single-Crystal Structure Refinement of $Ba_4In_8Sb_{16}$

empirical formula	$Ba_4In_8Sb_{16}$	vol (Å^3)	896.6(5)
fw	3415.92	*Z*	1
temp (K)	293(2)	density, ρ_{calc}, (g/cm^3)	6.327
wavelength (λ = Kα, Å)	0.71073	abs coeff (mm^{-1})	21.142
cryst syst	orthorhombic	no. of reflcns collcd	5906
space group	*Pnma*(No. 62)	data/restraints/params	1217/0/44
unit cell dimens (Å)	a = 10.166(3)	final R indices [$F_o^2 > 2\sigma(F_o^2)$][a]	R1 = 0.0449; wR2 = 0.1087
	b = 4.5239(14)	R indices ($F_o^2 > 0$)	R1 = 0.0744; wR2 = 0.1222
	c = 19.495(6)	largest diff peak and valley (e/Å^3)	2.974 and −1.904

[a] $R1 = [\Sigma||F_o| - |F_c||]/\Sigma|F_o|$. $wR2 = \{[\Sigma w(|F_o| - |F_c|)^2/[\Sigma w(F_o^2)^2]]\}^{1/2}$. $w = \sigma_F^{-2}$.

Table 2. Atomic Coordinates (×10^4) and Equivalent Isotropic Displacement Parameters (Å^2 × 10^3) for $Ba_4In_8Sb_{16}$

atom	*x*	*y*	*z*	*U*(eq)[a]
Ba(1)	7484(1)	2500	4550(1)	24(1)
In(1)	3770(2)	2500	7303(1)	24(1)
In(2)	6497(2)	−2500	6358(1)	21(1)
Sb(1)	4996(1)	2500	5977(1)	17(1)
Sb(2)	8974(1)	−2500	5702(1)	18(1)
Sb(3)	2056(2)	−2500	7251(1)	22(1)
Sb(4)	230(2)	2500	6419(1)	20(1)

[a] *U*(eq) is defined as one-third of the trace of the orthogonalized U_{ij} tensor.

initial positions of all atoms were obtained from direct methods. The structure was refined by full-matrix least-squares techniques with the SHELXTL[19] package of crystallographic program. Once all atoms were located, the occupancies of successive atoms were allowed to vary, but refinements did not lead to any significant change in the occupation factor. The final cycle of refinement performed on F_o^2 with 44 variables and 1217 averaged reflections converged to residuals wR2 ($F_o^2 > 0$) = 0.12. On the other hand, the conventional *R* index based on reflections having $F_o^2 > 2\sigma(F_o^2)$ was 0.0449. A difference Fourier synthesis calculated with phases based on the final parameters showed maximum and minimum peaks of +2.974 and −1.904 e/Å^3, respectively. The complete data collection parameters and details of structure solution and refinement results are given in Table 1. Final fractional atomic coordinates and displacement parameters are given in Table 2. More detailed crystallographic information, anisotropic displacement parameters, and a structure factor listing are available in the Supporting Information section.

Results and Discussion

Structure. The compound $Ba_4In_8Sb_{16}$ has a new structure type with two-dimensional character in which undulating puckered $(In_8Sb_{16})^{8-}$ anionic layers are separated with Ba^{2+} ions. The projection along the *b* axis illustrates a simplified view and shows small pentagonal tunnels composed of tetrahedral In and pyramidal Sb atoms; see Figure 1a. The building blocks of each pentagonal tunnel are $InSb_4$ tetrahedra and infinite Sb−Sb zigzag chains. All atoms in the structure lie on crystallographic mirror planes i.e., $z = {}^1/_4$ and ${}^3/_4$. The $InSb_4$ tetrahedra are arranged in rows that run parallel to the *b* axis direction. The tetrahedra share three Sb atom corners to make infinite chains, while the fourth corner of Sb atoms make a close approach to chemically equivalent Sb atoms of a neighboring infinite chain to make Sb−Sb bonds (between Sb(2) and Sb(4)) and thus produce infinite zigzag chains of Sb (Figure 2). This Sb−Sb coupling is responsible for the formation of the pentagonal tubes referred to above. Examples of similar $InSb_4$ tetrahedral units or analogous MPn_4 tetrahedra (M = Al, Ga; Pn = As, Sb), have been found in the structures of $Ca_{11}InSb_9$, $Ca_{11}GaAs_9$, and $Ca_{14}AlSb_{11}$,[20,21] where the tetrahedra are isolated, as well as in the structures of Ba_3AlSb_3, Ca_3AlSb_3, and $Ca_5Ga_2Al_6$ in which the tetrahedra are condensed. For example, in Ba_3AlSb_3,[22a,b] two $AlSb_4$ tetrahedra share a common edge, forming a dimeric anion $[Al_2Sb_6]$,$^{12-}$ while with a smaller counterion, as in Ca_3AlSb_3, an infinite chain $[AlSb_3]^{6-}$ made of two corner-sharing tetrahedra is formed.[22c] The single chains of $^1{}_\infty[AlSb_3]^{6-}$ can be further condensed via Sb−Sb bonding to form a double chain as found in $Ca_5In_2Sb_6$, $Sr_5In_2Sb_6$, and $Ba_5In_2Sb_6$.[23] Pnictido group 13 metalates with alkaline-earth-metal cations are expected to have higher dimensional structures than analogous group 14 compounds due to greater bonding requirements to fulfill the octet rule. Therefore, pnictido ligands in group 13 compounds might have more than two bonds depending on the alkali metal or alkaline earth metal, which would result in a higher dimensional network by edge sharing or corner sharing of tetrahedra. Highly condensed pnictido group 13 metalates with pyramidally bonded Sb ligands are found in $Na_2Al_2Sb_3$, $KGaSb_2$, and $KGaSb_4$.[24]

The Sb−In−Sb angles are in a range of 103.44−123.49°, which seems slightly wider than that observed in other compounds containing tetrahedra such as $Ba_5In_2Sb_6$, $Ca_5Al_2Sb_6$, and $Ba_5Al_2Bi_6$. The most deviated angle from the ideal tetrahedral angle is that of Sb(4)−In(1)−Sb(1) with 123.49°, which is responsible for the corrugation of the layer. The rest of the angles are close to those of other compounds with a $Ca_5Ga_2As_6$-type structure and the ideal tetrahedral angle of 109.4°. Therefore, the five-membered rings composed of two $InSb_4$ tetrahedra seem to be quite stable without severe strain in keeping the rings closed. Consequently, the five-membered rings have an envelope shape conformation rather than a planar shape, as shown in Figure 1b.

The distance between Sb(4) and Sb(3) is rather short at 3.34 Å although we do not consider it bonding. On

(19) Sheldrick, G. M. SHELXTL, Version 5; Siemens Analytical X-ray System, Inc.: Madison, WI, 1994.

(20) (a) *Structure and Bonding of Zintl Phases and Ions*; Kauzlarich, S. M., Ed.; VCH: New York, 1996. (b) Schafer, H.; Eisenmann, B. *Rev. Inorg. Chem.* **1981**, *3*, 29, 101

(21) (a) Cordier, G.; Schäfer, H.; Stelter, M. *Z. Naturforsch.* **1985**, *40B*, 868−871. (b) Brock, S. L.; Weston, L. J.; Olmsted, M. M.; Kauzlarich, S. M. *J. Solid State Chem.* **1993**, *107*, 513. (b) Cordier, G.; Schäfer, *Z. Anorg. Allg. Chem.* **1984**, *519*, 183.

(22) (a) Cordier, G.; Savelsberg, G.; Schäfer, H. *Z. Naturforsch.* **1982**, *37B*, 975−980. (b) Cordier, G.; Schäfer, H.; Stelter, M. *Z. Naturforsch.* **1985**, *40B*, 1100−1104. (c) Cordier, G.; Schäfer, H.; Stelter, M. *Z. Naturforsch.* **1984**, *39B*, 727−732.

(23) (a) Cordier, G.; Schäfer, H.; Stelter, M. *Z Naturforsch.* **1985**, *40B*, 5−8. (b) Cordier, G.; Stelter, M. *Z. Naturforsch.* **1988**, *43B*, 463−466. (c) Verdier, P. P.; L'Haridon, P.; Maunaye, M.; Laurent, Y. *Acta Crystallogr.* **1976**, *B32*, 726−728.

(24) (a) Cordier, G.; Ochmann, H.; Schäfer, H. *Rev. Chim. Miner.* **1984**, *21*, 282. (b)Cordier, G.; Ochmann, H.; *Z. Kristallogr.* **1991**, *195*, 306. (c) Cordier, G.; Ochmann, H.; *Z. Kristallogr.* **1991**, *195*, 308.

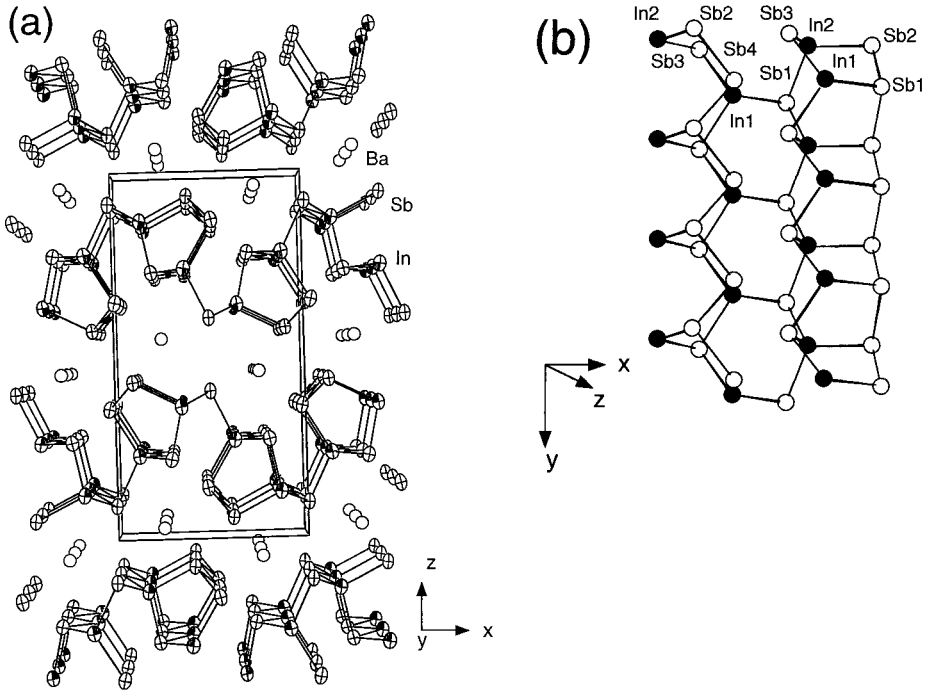

Figure 1. (a) ORTEP representation and labeling of $Ba_4In_8Sb_{16}$ viewed down the *b* axis with 80% probability thermal ellipsoids. (b) Different view showing the way pentagonal rings are connected.

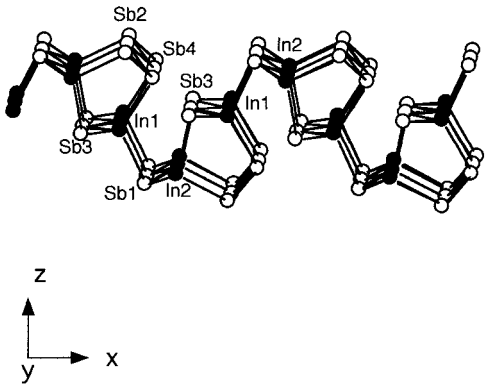

Figure 2. View of a $[In_8Sb_{16}]^{8-}$ layer with atomic labeling showing the chains of double In tetrahedra and zigzag Sb chains.

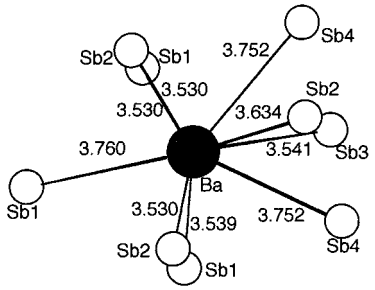

Figure 3. Coordination of the Ba (shaded) atom in $Ba_4In_8Sb_{16}$. The Sb atoms are labeled, and bond lengths between Ba−Sb are shown.

the basis of geometrical considerations, Sb(4) and Sb(3) are well positioned to be connected given a proper choice of counterion and main-group element. $Ba_4In_8Sb_{16}$ has two types of Sb atoms, one type being bonded to three In atoms and the other being associated with the Sb− zigzag chain. According to the Zintl concept, the formal charge of a four-bonded indium atom can be assigned as In^- and that of the three-bonded antimony atom can be assigned as Sb^0. The use of formal charge reflects the viewpoint that the bonding between indium and antimony atoms in anionic framework is covalent. On the basis of oxidation states, the three-coordinate Sb atoms can be assigned as Sb^{3-} ions and the Sb in Sb− Sb zigzag chains can be assigned as Sb^{1-}. The four-coordinate In atoms can be assigned as In^{3+}. Therefore, the formula is best represented as $[8(In^{3+})8(Sb^{3-})-8(Sb^{1-})]^{8-}$ The Ba^{2+} ions are found between the corrugated $(In_8Sb_{16})^{8-}$ layers and are coordinated by nine Sb atoms in a tricapped trigonal prismatic fashion (Figure 3). The Ba−Sb distances range from 3.53 to 3.760 Å, and are comparable to those found in related compounds.[19,20]

Electronic Structure. To understand the chemical bonding in this material, band structure calculations were performed on the anionic $(In_8Sb_{16})^{8-}$ sheets. The band structure was calculated using the extended-Hückel formalism with atomic orbital parameters of Table 4. Density of states (DOS) and crystal orbital overlap population (COOP) were calculated based on 516k points, and the results are shown in Figure 4a. The DOS plot contains total densities together with projections for the In p and Sb p orbital contributions. The projected DOS shows that the states near E_f are mainly contributions from In 5p and Sb 5p orbitals mixed with some corresponding s orbital character. The block of states at lower energy (<-16 eV) originates mainly from s orbitals of Sb. However, the s orbital states of the less electronegative In atoms contribute to the valence band and mix with p orbitals. This gives rise to sp^3 hybridization around the In atoms. The calculations show that there exists a direct energy gap suggesting the compound to be a semiconductor. Therefore, the band structure calculations also support $Ba_4In_8Sb_{16}$ to be structurally and electronically a Zintl

Table 3. Selected Bond Distances (Å) and Angles (deg) in $Ba_4In_8Sb_{16}$

In(1)−Sb(3) (×2)	2.857(2)	In(2)−Sb(3)	2.771(2)
Sb(4)	2.900(2)	Sb(1) (×2)	2.8282(14)
Sb(1)	2.871(2)	Sb(2)	2.825(2)
Sb(1)−In(2) (×2)	2.8281(14)	Sb(2)−In(2)	2.825(2)
In(1)	2.871(2)	Sb(4) (×2)	2.949(2)
Ba(1) (×2)	3.539(2)	Ba(1) (×2)	3.530(2)
Ba(1)	3.760(2)	Ba(1)	3.634(2)
Sb(3)−In(2)	2.771(2)	Sb(4)−In(1)	2.900(2)
In(1) (×2)	2.857(2)	Sb(2) (×2)	2.949(2)
Ba(1)	3.541(2)	Ba(1) (×2)	3.752(2)
Ba(1)−Sb(1) (×2)	3.530(2)	Sb(3)−In(1)−Sb(3)	104.69(8)
Sb(1) (×2)	3.539(2)	Sb(3)−In(1)−Sb(1) (×2)	103.44(5)
Sb(3)	3.541(2)	Sb(3)−In(1)−Sb(4) (×2)	110.05(5)
Sb(2)	3.634(2)	Sb(1)−In(1)−Sb(4)	123.49(5)
Sb(4) (×2)	3.752(2)	Sb(3)−In(2)−Sb(2)	105.08(7)
Sb(2)	3.634(2)	Sb(3)−In(2)−Sb(1) (×2)	111.60(5)
Ba(1) (×2)	4.5239(14)	Sb(2)−In(2)−Sb(1) (×2)	111.22(5)
		Sb(1)−In(2)−Sb(1)	106.22(7)
In(2)−Sb(1)−In(2)	106.22(7)	In(2)−Sb(4)−In(1)	95.21(9)
In(2)−Sb(1)−In(1)	89.84(5)	In(2)−Sb(4)−In(1)	95.21(9)
In(2)−Sb(1)−In(1)	89.84(5)	In(1)−Sb(4)−In(1)	105.05(14)
In(2)−Sb(2)−Sb(4)	99.87(5)	In(1)−Sb(6)−Sb(1)	100.67(9)
In(2)−Sb(2)−Sb(4)	99.87(5)	In(1)−Sb(6)−Sb(1)	100.67(9)
Sb(4)−Sb(2)−Sb(4)	100.17(7)	Sb(1)−Sb(6)−Sb(1)	100.31(12)

Table 4. Atomic Orbital Parameters[25] Used in Extended Hückel Calculations

atom	orbital	H_{ii} (eV)[a]	$\zeta 1$[b]	C1[b]
In	5s	−12.600000	1.903000	1.00000
	5p	−6.190000	1.677000	1.00000
Sb	5s	−18.799999	2.323000	1.00000
	5p	−11.700000	1.999000	1.00000

[a] $H_{ii} = \langle\chi_i|H^{\text{eff}}|\chi_i\rangle$, $i = 1, 2, 3, \ldots$. The value is approximated by the valence-state ionization potential. [b] Single-ζ STO's

phase. The valence and conduction bands are relatively wide with widths of about 7.5 and 6.5 eV, respectively. The broadening is due to extensive In−Sb and Sb−Sb interactions, which leads to a small band gap. Because of the weakness of this calculation method, the quantitative comparison with the experimentally observed value is not possible.

The projections for In−Sb and Sb−Sb bonds are shown in the COOP plots of Figure 4b. All the states below E_f are from In−Sb bonding interactions, consistent with maximized In−Sb bonding character. However, some of the Sb−Sb antibonding states just below the Fermi level are also filled, suggesting a slight weakening of bonding interactions in the Sb−Sb zigzag chain. Perhaps this fact explains the observed longer than average Sb−Sb distance of 2.949(2) Å, compared with the normal Sb−Sb bond distance (2.908(1) Å) in Sb metal, for example.

Thermal Stability and Spectroscopic Characterization. The compound $Ba_4In_8Sb_{16}$ is stable at room temperature in air; however, when heated at about 500 °C, it slowly decomposes to InSb and a barium-rich amorphous phase. The compound does not melt congruently. The X-ray powder pattern taken after DTA analysis indicated a mixture of InSb and $Ba_4In_8Sb_{16}$. A band gap was observed in the form of a broad absorption in the mid-IR region (4000−400 cm^{-1}) in the range 0.10−0.12 eV.

Charge Transport Measurements. To assess the thermoelectric properties of this material we conducted preliminary studies of the electrical conductivity and thermoelectric power of polycrystalline ingots of $Ba_4In_8Sb_{16}$ as a function of temperature. The conductivity

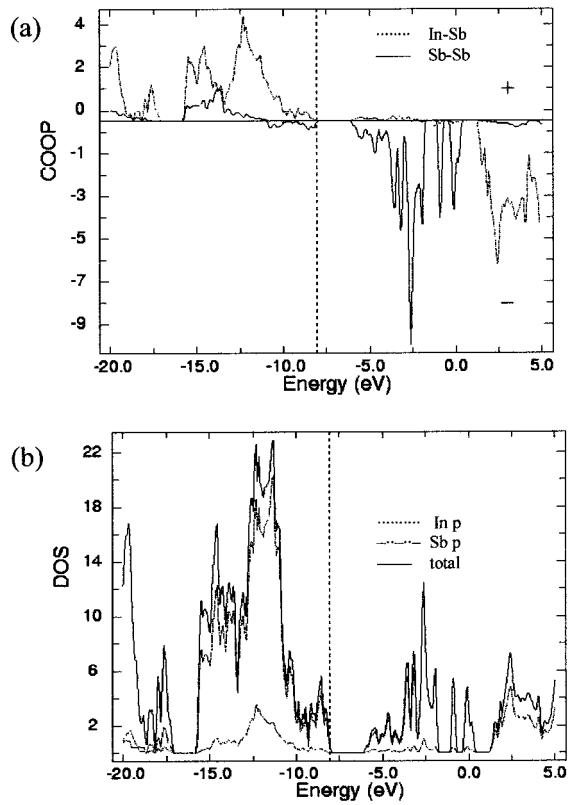

Figure 4. COOP and DOS curves for $Ba_4In_8Sb_{16}$: (a) COOP curves of Sb−Sb (solid line) and In−Sb(dotted line) interaction; (b) DOS and projected DOS curves. The projection of In 5p (dotted line), Sb 5p(double dotted line), and total DOS (solid line) curves are shown.

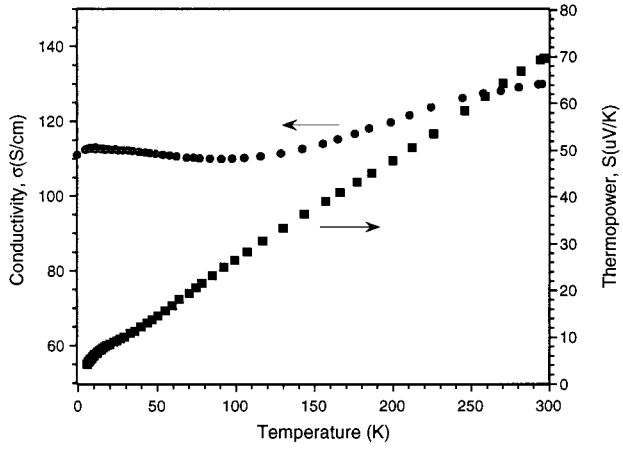

Figure 5. Temperature dependence of the electrical conductivity and thermoelectric power (Seebeck coefficient) for a polycrystalline ingot of $Ba_4In_8Sb_{16}$.

at room temperature was ∼135 S/cm and did not vary greatly with temperature; see Figure 5. This is consistent with a narrow-gap semiconductor behavior. The electrical conductivity of $Ba_4In_8Sb_{16}$ is relatively low compared to the values of well-known semi-metals such as Bi_2Te_3 (2.2×10^3 S/cm).[26] It is comparable to the

(25) (a) Wolfsberg, M.; Helmholz, L. *J. Chem. Phys.* **1952**, *20*, 837. (b) Ballhausen, C. J.; Gray, H. B. *Molecular Orbital Theory*; Benjamin: New York, 1965. (c) Basch, H.; Viste, A.; Gray, H.; *Theor. Chim. Acta* **1965**, *3*, 458. (d) Basch, H.; Viste, A.; Gray, H.; *J. Chem. Phys.* **1966**, *44*, 10. (e) Baranovskii, V.; Nikolskii, A. *Theor. Eskp. Khim.* **1967**, *3*, 527.

(26) Rosi, F. D.; Abeles, B.; Jengen, R. V. *J. Phys. Chem. Solids* **1959**, *10*, 191.

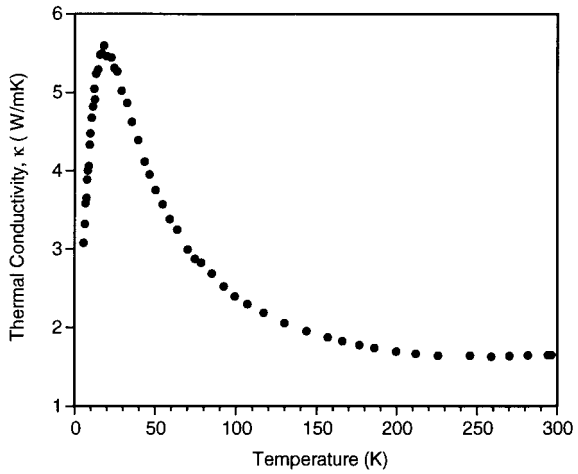

Figure 6. Temperature dependence of the thermal conductivity of a polycrystalline ingot of $Ba_4In_8Sb_{16}$.

values observed in some of the bismuth chalcogenides we described earlier: $K_{2.5}Bi_{8.5}Se_{14}$ (150 S/cm), β-$K_2Bi_8Se_{13}$ (240 S/cm), and $BaBiTe_3$ (42 S/cm).[4]

The value of thermoelectric power S (Seebeck coefficient) for $Ba_4In_8Sb_{16}$ was about +70 μV/K at room temperature and showed a linear decrease with decreasing temperature. The positive value of thermoelectric power indicates that $Ba_4In_8Sb_{16}$ is a p-type (hole) semiconductor. On the basis of the computed band structure discussed above the holes in this material reside primarily in the Sb sublattice. One has to keep in mind that these values of electrical conductivity and Seebeck coefficient are not intrinsic to the material but instead reflect a given doping state. The values could likely be improved with better sample morphology and appropriate choices of dopants and dopant concentrations.

Thermal Conductivity. Low thermal conductivity is one of the key requirements for a useful thermoelectric material. Indeed the most interesting aspect of our investigation is the magnitude of the total thermal conductivity (κ) of $Ba_4In_8Sb_{16}$. Figure 6 shows κ as a function of temperature. The total thermal conductivity is about 1.7 W/m·K at room temperature, which is comparable to the value of optimized Bi_2Te_3 alloy (1.4−1.6 W/m·K). The electronic thermal conductivity at 300 K is no more than about 5% of the total thermal conductivity and is even a smaller fraction at lower temperatures. This we base on the values of the electrical conductivity and invoking the Wiedemann−Franz law. Despite an obviously short phonon mean-free path, the overall character of the thermal conductivity is that of a crystalline dielectric solid. An inspection of the atomic displacement parameter of Ba^{2+} ion in Table 2 indicates that it is very comparable to those of the other atoms in the structure. From this, we can conclude that not much "rattling" motion of Ba atoms is occurring in $Ba_4In_8Sb_{16}$ indicative of a snag fit of Ba atoms in their cavity.[10] Therefore, the total thermal conductivity is primarily due to the low symmetry and dimensionality of the structure as well as presence of heavy atoms. Because of the lack of thermoelectric data for other Zintl compounds, a thorough comparison was not possible. However, the thermoelectric properties of $Ba_4In_8Sb_{16}$ reported here are encouraging and suggest a new category of possible thermoelectric materials in other similar Zintl phases. Efforts to fully characterize the thermoelectric properties as a function of various dopants are now underway.

We believe the total thermal conductivity can be driven to be even lower by preparing solid solutions of the type $Ba_{4-x}Sr_xIn_8Sb_{16}$. A "rattling" motion of the smaller Sr atoms, in cavities designed for Ba atoms, could cause additional heat carrying phonon scattering thereby further frustrating heat transport in this material.

In conclusion, we have synthesized a new Zintl phase, with unique corrugated layers and a narrow band gap. Until recently, research on Zintl type compounds concentrated predominantly of exploring the extent of the validity of the concept itself and as such focused mainly on systems with relatively light atoms in the framework. Most currently known Zintl phases are air and moisture sensitive. However, the analogues with heavier elements, if environmentally stable, could be those with useful potential applications. The structural complexity of $Ba_4In_8Sb_{16}$ is reminiscent of those found in many ternary A/Bi/Q phases.[4] Many more Zintl type phases with heavy main-group atoms and narrow band gaps are anticipated. This area of solid state chemistry presents itself as a potentially rich field in which to search for new thermoelectric compounds.

Acknowledgment. Financial support from DARPA through the Army Research Office (DAAG55-97-1-0184) and the Center for Fundamental Materials Research are gratefully acknowledged. The work at the University of Michigan is supported by DARPA through the Office of Naval Research. S.-J.K. acknowledges financial support from the Korean Science and Engineering Foundation (96-0501-0601-3) and the Yonam Foundation of Korea.

Supporting Information Available: Tables giving more detail on crystallographic data and anisotropic displacement parameters as well as structure factors This material is available free of charge via the Internet at http://pubs.acs.org.

CM990237Y